Archeologia e Calcolatori
37.1, 2026, 277-294
doi 10.19282/ac.37.1.2026.14

ASSESSING CULTURAL HERITAGE ARTIFACTS THROUGH QUANTITATIVE METHODS: INSIGHTS FROM CORINTHIAN ROMAN CAPITALS

1. Introduction

A quantitative assessment of cultural heritage artifacts represents an important methodological advancement in the study and management of the material past. Traditionally, the analysis and classification of archaeological objects – especially architectural decoration – have relied primarily on qualitative observation and the expertise of specialists. While this interpretative approach remains fundamental, the introduction of quantitative methods makes it possible to complement traditional scholarship with measurable, reproducible parameters. By translating formal and stylistic features into numerical data, researchers can compare large sets of artifacts in a systematic way, identify patterns that might otherwise remain unnoticed, and test hypotheses about chronology, production techniques, and workshop organization.

Beyond its scholarly implications, the quantitative analysis of cultural heritage has practical applications in documentation, conservation, and heritage management. Digital and computational tools allow artifacts to be recorded, analysed, and shared more efficiently, facilitating collaboration among institutions and enabling the study of collections that are geographically dispersed. In contexts where cultural heritage is threatened – whether by conflict, environmental factors, or urban development – quantitative approaches can also support rapid documentation and monitoring efforts. More broadly, the development of rigorous analytical frameworks contributes to the long-term preservation and understanding of cultural heritage, reinforcing its value as a shared resource for research, education, and society.

In this article we focus specifically on ancient Roman Corinthian capitals. Their typologies have been extensively studied, and several formal features have been identified for the classification and dating of these artifacts. In particular, the distinct sharpness of the acanthus leaves has long been recognized as a significant element of analysis in archaeological research, as it underwent notable transformations throughout Roman history. Nevertheless, traditional approaches to the study of these capitals rely largely on the visual assessment and expertise of specialists, while a systematic quantitative method for describing and comparing such stylistic features has yet to be fully explored.

Mathematical morphology (Heijmans 1995; Hÿtch, Hawkes 2020) is a framework for image processing and feature extraction applicable to grayscale images, and especially relevant when an object contour can be estimated (Leymarie, Levine 1989, 1993; Hossain, Chen 2019). Quantitative morphological methods were considered in archaeology for the estimation of geometrical features and landmarks in artifacts (Bello, Soligo 2008; Herzlinger *et al.* 2017). However, the problem of image segmentation becomes challenging when many intersecting objects are considered, and this is the case of the 2D drawings of Roman capitals considered here, where several architectural elements are drawn together with continuity. Machine learning methods of image segmentation (Ghosh *et al.* 2020) could potentially be developed for this task, however that would require a large set of training data of segmented capitals images which is to us unavailable at present.

In this paper, aiming for a quantitative description of the shapes' sharpness in Corinthian Roman capitals, we propose the mathematical curvature as the relevant observable. For its estimation we introduce a local approximation integral based on a single spacescale parameter which governs the locality-precision tradeoff. This coarse-grained approach does not require training data, and also does not require regressions or optimizations beyond the four parameters fixed in the image preprocessing, and of a topological filtering stage to select for curves and discard intersections and noise. Motivated by the applicability on archaeological drawings, we provide the Python implementation of this method, offering a new tool for architectural historians and researchers working in the field of the tangible cultural heritage (Grosman 2016; Morgan 2022).

2. Archaeological background

In broad terms, the typological and stylistic development of the Roman Corinthian capital can be summarized over a long chronological span extending from the final decades of the first century BCE to approximately the fourth century CE. This synthesis provides a functional framework for the present study, which focuses specifically on the canonical form of the Corinthian capital as it developed within the Roman architectural tradition. For the purposes of clarity and methodological consistency, the analysis is limited to the so-called normal Corinthian capital, thereby excluding other related but distinct variants such as the Italic capital and the so-called Corinthianising capital. These latter types present a wide range of formal variations and frequently employ different configurations of the acanthus leaves, making them less suitable for a controlled comparative analysis.

The scope of the study is also geographically circumscribed. Attention is directed primarily to capitals produced in the city of Rome and in neighbouring urban centres closely connected to the capital's artistic and architectural milieu. At the same time, the framework also includes works that can be directly linked to Roman models through the activity of imperial workshops or through the major provincial monumental programs promoted under imperial patronage. By focusing on this relatively coherent cultural and stylistic environment, it becomes possible to trace the gradual transformation of ornamental features – particularly the morphology of the acanthus leaves – within a historically meaningful sequence, providing a solid basis for the quantitative analysis proposed in this study.

The development of the capital with *acanthus mollis* called by German scholars Normaltypus has its canonical formulation in the capitals of the Mars Ultor temple in the Augustus forum in Rome (Heilmeyer 1970, 25-31). The type maintains a relatively constant general pattern for more than two centuries, until the end of the Severan dynasty, with a few sporadic examples dating to the mid-3rd century CE. In the late Hadrianic period, in addition to capitals with *acanthus mollis*, an *acanthus spinosus* type appears, produced in early times by craftsmen from Asia Minor (Heilmeyer 1970, 165-172; Freyberger 1990, 125-129). From the Severan age the Corinthian-Asian capital is common both in Rome and in various centers in Italy, and during the third century supplanted the *acanthus mollis* type to become in turn the canonical form throughout the Late Antiquity. Within this dual path, we can identify in both variants some moments of rupture, marking the emergence of new forms. In the few decades between the second Triumvirate and the early Augustan age a type of capital (Fig. 1) is easily recognizable by the vertical sequence of a drop-shaped eyelet followed by one or two triangular eyelets (Heilmeyer 1970, 36-42). Widespread mainly in Rome, Italy, and *Gallia Narbonensis*, it can be considered an anticipation of the normal Corinthian capital in that it combines the pointed-ended leaflets of the *acanthus spinosus* with the concave lobes of the *acanthus mollis*. The type is short-lived: in the mid-Augustan age (Fig. 1) the capitals from the Augustus Forum testify to the emergence of the so-called Normalkapitell, whose constituent elements are leaves with spoon-shaped lobes, each formed by three/four leaflets with concave section and rounded ends, fluted caules, axial stem supporting the abacus flower, helices and volutes with canal (Heilmeyer 1970, 25-31). Until the end of the Julio-Claudian age and the beginning of the Flavian age the type retains its original formal characteristics, evolving in depth dimension, as shown by the leaves of a series of capitals from the Neronian age (Heilmeyer 1970, 133-134).

A clear stylistic caesura is recorded under Domitian, when a type, called by K. Freyberger Grundmuster I (Fig. 1) (Freyberger 1990, 5-33), which changes the leaf to a more rigid structure, accentuating the central rib, is imposed in the main monuments of Rome; the type probably dates back to an original created in one of the workshops engaged in the imperial monumental programs. With the Trajanic Forum another type, the so-called Grundmuster II, appears (Freyberger 1990, 43-48), created presumably

Fig. 1 – Upper left: Corinthian capital, Rome, Palatine, Temple of Apollo (from Heilmeyer 1970, tav. 6.3); upper center: Corinthian capital, Rome, Forum of Augustus, Mars Ultor Temple (from Heilmeyer 1970, tav. 2.1); upper right: Corinthian capital, Rome, Forum of Nerva, 'Colonnacce' (from Freyberger 1990, tav. 1a); lower left: Asiatic Corinthian capital, Ostia, Forum Baths, Frigidarium (Pensabene 1973, n. 333, tav. XXXII); lower right: Asiatic Corinthian capital, Ostia, Decumanus Maximus (Pensabene 1986, 317, fig. 5c).

for the occasion a few decades later. The latter transforms the acanthus into an even more stylized form and accentuates the vertical dimension of the structure. Throughout the second century the two types mentioned remain essentially unchanged, while the Severan age is characterized by an eclectic use of both models (Freyberger 1990, 97-108).

The introduction of the Asiatic Corinthian capital is one aspect of the spread of the Asiatic architectural sculpture and decoration, documented from the Late Hadrianic period first in Rome, and then elsewhere. In the earliest capitals, such as these in the Forum Baths in Ostia (Fig. 1) (Pensabene 1973, 94, nn. 332-333; n. 306, fig. 1a) the traditional pattern is maintained. The type however soon evolves into a simplification of the decorative apparatus, which in the later phase becomes radical, and into the reduction of the leaves to pure graphic form. Already in the capitals of the Severan age the *acanthus spinosus* becomes a geometric fan, and the cauliculus is reduced to a triangular scale (Pensabene 1986, 306-309; Freyberger 1990, 126-129, fig. 1b). The stylisation becomes more pronounced in the period of military anarchy, and in the decades between the end of the third century and the Constantinian age the apparatus atrophies to such an extent (Fig. 1) (Pensabene 1986, 312-319) that the helices are reduced to horizontal tongues until they almost disappear, thus anticipating some outcomes of Byzantine production (Kautzsch 1936, 5-115; Pensabene 1986, 352-355; Kramer 1997; Pralong 2000, 85-89). It is clear that this late production is better suited for accurate reading by the computational method, as the three-dimensionality of the carved decoration has largely disappeared.

3. The curvature estimation method

3.1 *Frame cut*

The raw image, typically an archaeological drawing, is converted to a grayscale image and represented as a Python numpy array with values in [0,1]. Let us denote by $\mathbf{x}$ the spatial locations and by $\tilde{y}(\mathbf{x})$ their corresponding intensity. The frame is cut according to a small positive lower threshold on the intensity so to keep only a minimal whitespace around the relevant section of the image where the drawing is located.

3.2 *Projection to a mask*

The grayscale image undergoes Laplacian smoothing with parameter c_L in order to collapse the background coloring lines into smooth plateaus, and for the raw lines to become rounded ridges. Then the smoothed y_s is normalized through $y_s' = y_s - \min y_s + \epsilon_L \text{ Std } [y_s]$ and $y = y_s'/\max(y_s')$, where Std denotes standard deviation and the floor with parameter is applied to prevent numerical issues with logarithms. The resulting $y(\mathbf{x})$ is then projected to a Boolean array, i.e. the mask, as a product of the three below thresholds:

- $y > c_0$: a lower bound on the grayscale intensity to filter the background noise.
- $||\nabla_{\mathbf{x}} \log(y)||^2 < c_1$: an upper threshold on the squared log-gradient to reduce the thickness of the resulting curves. Indeed rounded ridges have zero gradient on the perpendicular direction to the local segment only on the top, while variations on the parallel direction should be slower. For the threshold to work on curves of different intensities, the logarithm is taken to consider relative variations.
- $\nabla_{\mathbf{x}}^2 \log(y) < -c_2$: a negative upper threshold on the Laplacian to select for the rounded ridges.

The four parameters (c_L, c_0, c_1, c_2), which are all taken to be positive, have been tuned for a single set to work for the whole set of curves in our two archaeological applications. In general, their values should be tuned to select for the relevant shapes where the curvature is to be estimated. Here the decision to filter out the background coloring lines is motivated by our understanding of the archaeological drawings. In particular, the drawings aim to convey the 3D spatial depth through the background coloring, therefore such lines do not represent actual shapes but rather the role of shadows. Also we note that the archaeological drawings' representation of depth is not precise enough for us to estimate the 3D shapes, therefore we neglect this aspect for the curvature estimation.

We wish to quantify the curvature of the shapes observed in the mask $m(\mathbf{x})$. The points $\mathbf{x}$ in the grid where $m(\mathbf{x}) = 1$ are hereafter referred to as mask points. Only for these mask points we perform the below local curvature estimation, while the other points are not considered. For computational efficiency, this estimation is based on a smaller local submask centered in $\mathbf{x}$, that means to neglect interactions of longer distance than effectively needed by the below curvature definition.

3.3 *Topological conditions*

We first filter for the connected region of mask points in the submask which includes the center $\mathbf{x}$, while other regions are removed from the local submask. This is implemented with a discrete diffusion equation on the submask topology: starting from a discrete Delta distribution in the center, the reached points with positive density after enough iterations of the discrete Laplacian is the new domain. Let us denote this filtered submask centered in $\mathbf{x}$ as $\mathbf{x}\ \ \widetilde{m}_{\mathbf{x}}(\mathbf{y})$, where $\mathbf{y}$ is the relative displacement vector from $\mathbf{x}$.

The derived submask, which is composed of a single connected region of mask points by construction, is studied to determine if the topology of such region is compatible with that of a curve. After checking if the region size is large enough to be considered a signal and not just some dots noise resulting from the above mask projection, the curve topology requirement is studied by temporarily removing a small round neighbourhood of mask points around the center and checking that the number of connected regions becomes exactly two, meaning that the curve has been broken in two pieces. This is implemented by the Python package 'scikit-image.measure' which identifies the connected regions. In order to avoid the asymmetry deriving from finite length curves to dominate the below integrals, we require such two pieces to be of comparable sizes $(s_1,\ s_2)$ by introducing a threshold M to filter $[\ln(s_1/s_2)]^2 < M$. If the above topological conditions are met, we proceed to estimate the local curvature for the point $\mathbf{x}$ from the normalized submask $m_{\mathbf{x}}(\mathbf{y}) \equiv \widetilde{m}_{\mathbf{x}}(\mathbf{y}) / \int d\mathbf{y}\, \widetilde{m}_{\mathbf{x}}(\mathbf{y})$.

3.4 *The local curvature estimation integral*

Given the local submask $m_{\mathbf{x}}(\mathbf{y})$, instead of explicitly parametrizing a curve to it, we introduce an approximate estimation integral for the local curvature vector,

$$\mathbf{C}(\mathbf{x}) = \frac{4\beta}{3Z(\mathbf{x})} \int d\mathbf{y} ||\mathbf{y}||^2 e^{-\beta||\mathbf{y}||^2} m_{\mathbf{x}}(\mathbf{y})\, \mathbf{y}, \tag{1}$$

with normalization $Z(\mathbf{x}) = \int d\mathbf{y}\, ||\mathbf{y}||^2 e^{-\beta||\mathbf{y}||^2} m_{\mathbf{x}}(\mathbf{y})$. The prefactor is chosen for this definition to converge to the inverse radius of curvature in a special noiseless case as discussed in the following subsection. This definition is based on the inverse spacescale parameter β which should capture the typical observation length where individual angled or curved shapes are visible. The tradeoff in β comes from the noise and discreteness of the mask for short spacescales $\beta \to \infty$ and the appearance of multiple inflection points at long spacescales $\beta \to 0$. The optimal spacescale β is to be empirically fine-tuned on the samples under study. We note that the approximation integral of Eq. (1) could in principle be the solution of a convex optimization involving the parametrization of the curve with respect to some objective function. Not knowing that particular objective function, we at least require the integral of Eq. (1) to satisfy some desirable properties like the convergence to the correct curvature vector in the noiseless limit of a plane curve of vanishing width in the limit $\beta \to \infty$.

We define the global curvature as the average over the mask of the absolute local curvature, $C \equiv \int d\mathbf{x}\, m(\mathbf{x})\, ||\mathbf{C}(\mathbf{x})|| \,/ \int d\mathbf{x}\, m(\mathbf{x})$.

Let us note that, were the geometric shapes not smooth curves but angles, the mathematical curvature is not defined and the integral of Eq. (1) would diverge with $\sqrt{\beta}$ as shown below. In practice, we work with a finite β and the width of the segments together with the smoothing done in the mask estimation phase are such that such divergence is not observed.

3.4.1 *Relation to the radius of curvature*

The absolute value of the approximation integral of Eq. (1) converges to the inverse of the radius of curvature in the noiseless case in the limit of a vanishing spacescale $\beta \to \infty$. We show this by considering a circle of radius R centered in $(0, R)$, which is given by the Pythagorean relation $(R - x_2)^2 + x_1^2 = R^2$. Solving for x_2 and considering only the lower semicircle solution we get $x_2 = R - \sqrt{R^2 - x_1^2}$. Expanding the square root to second order, the parabola equation which approximates the semicircle for small $|x_1| \ll R$ is $x_2 = x_1^2/(2R)$. Assuming the width of the parabola as a plane curve to be vanishing but constant along the curve, we can represent the mask as a Dirac delta density with respect x_2 to centered in $x_1^2/(2R)$ multiplied by the arc length factor $\sqrt{1+\left(\frac{dx_2}{dx_1}\right)^2} = \sqrt{1+\left(\frac{x_1}{R}\right)^2}$, $m(\mathbf{x}) = \delta_2\left(x_2 - \frac{x_1^2}{2R}\right)\sqrt{1+\left(\frac{x_1}{R}\right)^2}$.

The approximation integral of Eq. (1) evaluated $\mathbf{x} = \mathbf{0}$ in with this mask density is

$$\frac{3Z(\mathbf{0})}{4\beta}\mathbf{C}(\mathbf{0})$$

$$= \int\int dy_1 dy_2\,(y_1^2 + y_2^2)\,e^{-\beta(y_1^2+y_2^2)}$$

$$\times\,\delta_2\left(y_2 - \frac{y_1^2}{2R}\right)\sqrt{1+\left(\frac{y_1}{R}\right)^2}\,(y_1, y_2)$$

$$= \int dy_1\left(y_1^2 + \frac{y_1^4}{4R^2}\right)e^{-\beta\left(y_1^2+\frac{y_1^4}{4R^2}\right)}\sqrt{1+\left(\frac{y_1}{R}\right)^2}\left(y_1, \frac{y_1^2}{2R}\right).$$

The first component in zero being the integral of an odd function, $C_1(\mathbf{0}) = 0$, and it was expected since the curvature points towards the center of the circle which we put on the x_2 axis. In the limit $\beta \to \infty$ the observational spacescale vanishes and $|y_1|/R \to 0$, so that the higher order terms in $|y_1|/R$ become negligible and the integral becomes, to leading order,

$$\frac{3}{4\beta}Z(\mathbf{0})C_2(\mathbf{0}) \approx \int dy_1\,e^{-\beta y_1^2}\,\frac{y_1^4}{2R} = \frac{3\sqrt{\pi}}{8R\beta^{\frac{5}{2}}}. \tag{2}$$

In the same limit we obtain $Z(\mathbf{0}) \approx \int dy_1\,y_1^2 e^{-\beta y_1^2} = \frac{\sqrt{\pi}}{2\beta^{\frac{3}{2}}}$, and from Eq. (2) this implies the approximation integral to converge to the oriented curvature, $\mathbf{C}(\mathbf{0}) = \left(0, \frac{1}{R}\right)$, and its absolute value to the inverse of the radius of curvature. We note that this limit would still hold if we were to multiply the integrand in the local curvature of Eq. (1) by higher order terms of the form $1 + a||\mathbf{y}||^b$ with $a \in \mathbb{R}$ and $b > 0$.

Given the arbitrary units of the drawings, the estimation of the local radius of curvature and its comparability relies on their style to be uniform across samples. Indeed, a rescaling of the spatial units would proportionally affect R, so that a standardization in the representation was needed and motivated the choice of the archaeological drawings.

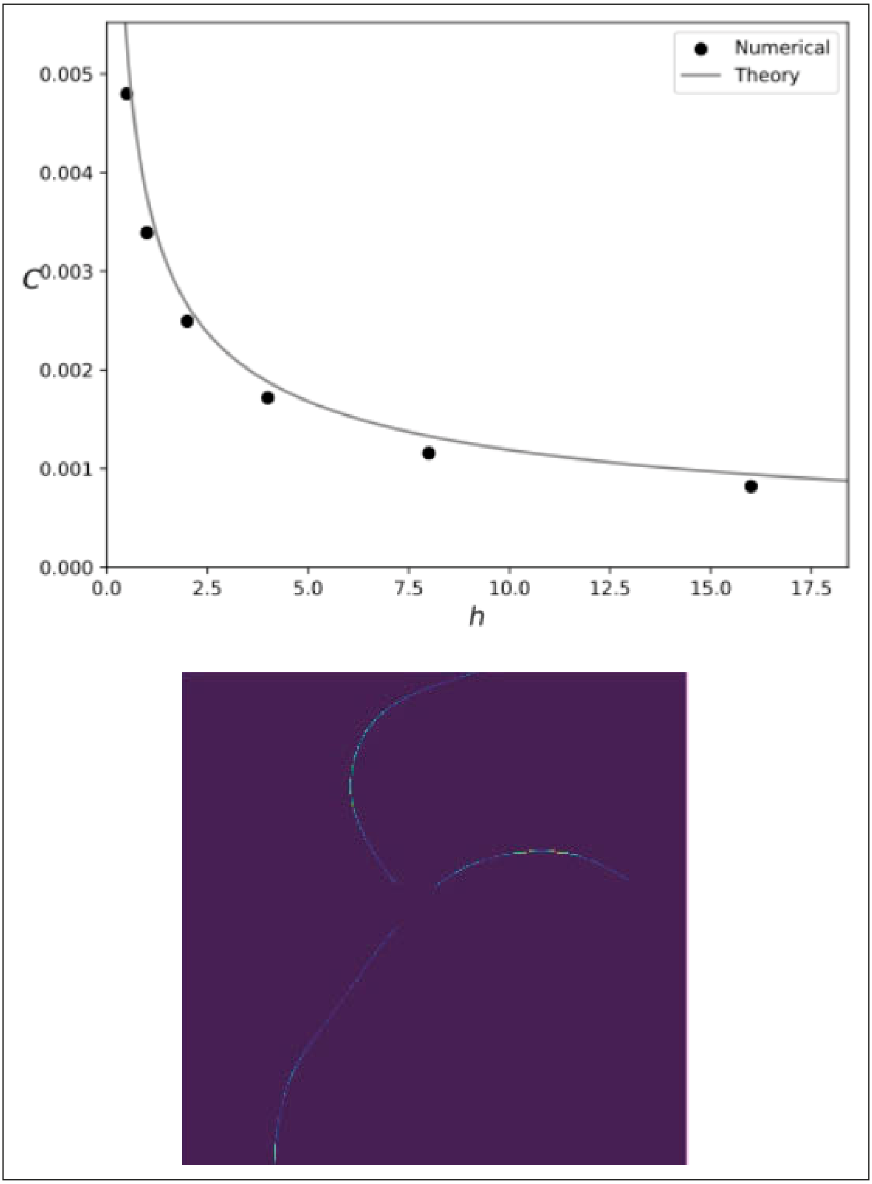

Fig. 2 – Testing the method on simple stochastic curves generated by a particle undergoing underdamped rotational diffusion, see Eq. (3). Left, dependence of the average estimated curvature as a function of the rotational relaxation parameter h, compared with the corresponding analytical result for $\beta \to 0$ on zero-width curves; right, example of one of such generated stochastic images with the coloring proportional to the algorithm-estimated local absolute curvature $||\boldsymbol{C}(\boldsymbol{x})||$, here with $h = 1$.

3.4.2 Divergence for exact angles

Consider a plane curve describing an angle θ with vertex in $\mathbf{0}$ and the x_2 axis as angle bisector. This can be written as a function $x_2 = \alpha|x_1|$ with $\alpha \equiv \tan^{-1}(\theta/2)$. Considering the arc length factor $\sqrt{1+\left(\frac{dx_2}{dx_1}\right)^2} = \sqrt{1+\alpha^2}$ we write it as a 2D density

$$m(\mathbf{x}) = \delta_2(x_2 - \alpha|x_1|)\sqrt{1+\alpha^2}.$$

The approximation integral of Eq. (1) evaluated in $\mathbf{x} = \mathbf{0}$ with this mask density is

$$\begin{aligned}
&\frac{3Z(\mathbf{0})}{4\beta}\mathbf{C}(\mathbf{0}) \\
&= \int\int dy_1 dy_2\, (y_1^2 + y_2^2)\, e^{-\beta(y_1^2+y_2^2)}\, \delta_2(y_2 - \alpha|y_1|)\sqrt{1+\alpha^2}\,(y_1, y_2) \\
&= (1+\alpha^2)^{\frac{3}{2}}\int dy_1\, y_1^2\, e^{-\beta(1+\alpha^2)y_1^2}\,(y_1, \alpha|y_1|) \\
&= \left(0, \frac{\alpha}{\beta^2\sqrt{1+\alpha^2}}\right).
\end{aligned}$$

Similarly, we obtain $Z(\mathbf{0}) = \frac{\sqrt{\pi}}{2}\beta^{-\frac{3}{2}}$, and then for the curvature

$$C_2(\mathbf{0}) = \frac{8}{3\sqrt{\pi}}\frac{\alpha}{\sqrt{1+\alpha^2}}\sqrt{\beta},$$

which diverges as $\sqrt{\beta}$ for small spacescales $\beta \to \infty$. For finite β the curvature is instead bounded as indeed in the limit of a small angle $\theta \to 0$ the curvature converges to $\frac{8}{3\sqrt{\pi}}\sqrt{\beta}$.

4. Applications

4.1 *Numerical tests*

We first test the algorithm on a set of numerically generated drawings. These are sampled from random trajectories of a particle with constant velocity v and angular direction $\mathbf{e^{i\theta}} \equiv [\cos(\theta), \sin(\theta)]$ fluctuating according to the underdamped (Risken 1996) equations

$$\begin{cases} \frac{d\theta}{dt} = \dot{\theta} \\ d\dot{\theta} = -h\dot{\theta}dt + \sigma dW, \end{cases}$$

where $h > 0$ an $\sigma > 0$ are parameters and dW are standard Brownian motion increments (Karatzas and Shreve 1991). The equation for $\dot{\theta}$ is the well-known Ornstein-Uhlenbeck process whose stationary density is given by the normal distribution $\mathcal{N}\left(0, \frac{\sigma^2}{2h}\right)$. The local absolute value of the curvature is here given by $\frac{1}{v}\left|\frac{d\theta}{dt}\right| = 1/R$. The total curvature will then be given by the expectation $\mathbb{E}[1/R] = \frac{1}{v}\mathbb{E}\left[\left|\frac{d\theta}{dt}\right|\right] = \frac{\sigma}{v\sqrt{\pi h}}$. We test our algorithm by verifying this formula on the numerically generated drawings (Fig. 2).

4.2 *Background curvature*

The curves in the drawings have a finite width which results in a background curvature. In other words, if a drawing of a straight line is digitized in a way that its width comprises more than one pixel, then it will result to have some small nonzero curvature according to Eq. (1), as shown below. This issue, unavoidable at finite resolution, can be tackled by subtracting from the computation the background curvature $C(\sigma = 0)$, defined as the curvature of a straight line with the same width of the ones in the original drawings. This background curvature is estimated numerically

Fig. 3 – Illustration of the curvature estimation procedure on a drawing by P. Pensabene of a column capital from the theatre of Ostia, dated around 12 BCE (Pensabene 1973, tav. LXXX, n. 204). Left: section of the archaeological drawing of the artifact. Center: the corresponding mask derived from the density, gradient and Laplacian thresholds. Right: the estimated local curvature with higher values in brighter colour. The colour normalization is done with respect to this figure maximum. As expected, it is more pronounced on the edges and angles.

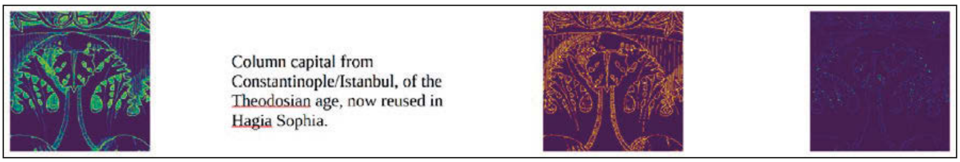

Fig. 4 – Same as Fig. 3, but for a more recent artifact with an accordingly higher value of the curvature. Drawing taken from Zollt 1994, fig. 22, n. 617, of a column capital from Constantinople/Instanbul, of the Theodosian age, now reused in Hagia Sophia Grand Mosque.

on the underdamped example of Eq. (3) by setting $\sigma = 0$. To have an idea of the impact of the background curvature, let us consider a straight line coincident with the x_1 axis which can be represented by the mask density $m(\mathbf{x}) = \delta_2(x_2)$, where δ_2 denotes the Dirac delta in two dimensions. The apparent curvature of this line when evaluated from a point at distance ϵ is

$$\frac{3Z(-\epsilon\widehat{x_2})}{4\beta}\mathbf{C}(-\epsilon\widehat{x_2})$$

$$= \int\int dy_1 dy_2\, (y_1^2 + y_2^2)\, e^{-\beta(y_1^2+y_2^2)}\, \delta_2(y_2 - \epsilon)\, (y_1,\, y_2)$$
$$= \int dy_1\, y_1^2\, e^{-\beta y_1^2}\, (y_1,\, \epsilon) + \mathcal{O}(\epsilon^3) = \big(0,\, \epsilon Z(-\epsilon\widehat{x_2})\big) + \mathcal{O}(\epsilon^3),$$

where the last line equalities are valid to leading order, and it implies that $C(-\epsilon\widehat{x_2}) = \frac{4}{3}\beta\epsilon$. The term $\widehat{x_2}$ denotes the unit vector along the x_2 axis. The apparent curvature of a straight line is then expected to be impacted from local contributions of order $||\mathbf{C}(\mathbf{x})|| \approx \beta\epsilon$ where is ϵ the line width in pixels.

5. Selection of the case studies

The selection of the case studies was guided by the clarity and distinctiveness of specific ornamental features, particularly the acanthus leaves. The first case study consists of an archaeological drawing of a column capital dated to 12 BCE from the theatre of Ostia, an important Roman site known for its well-preserved architectural elements. The second case study is a column capital from the 5th century CE, currently reused in the church of St. Sophia in Constantinople (modern-day Istanbul). These capitals were chosen due to the sharpness and definition of their acanthus leaf carvings, a characteristic that makes them especially suitable for comparative analysis. Despite the distinctiveness of this feature, recognizing and interpreting it accurately often requires specialized knowledge.

5.1 *Results on the selected examples*

We applied the described method to the two archaeological drawings discussed above. The results are shown in Figs. 3-4. As expected, the second capital has an average squared curvature larger than the first (around 25% more), as expected from the stylistic considerations above. The plot of the local curvature shows that the algorithm is correctly identifying angles and regions of high local curvature. We note that the background curvature described above and that was considered in Fig. 2 for the testing of the algorithm, cannot be estimated here in this archaeological application where the curve widths are not a constant. However, this baseline should not impact the curvature difference between the two samples when their line style representation is similar.

5.2 *Numerical implementation details*

The curvature estimation method was implemented in Python, leveraging a suite of open-source libraries optimized for efficient image processing and large-scale numerical computations. High-resolution archaeological drawings (processed as large TIFF images) are ingested using the Pillow (PIL) library, while matrix manipulations – involving arrays of up to 2500×2500 pixels – are performed using NumPy.

To simulate the continuous Laplacian smoothing required for the mask projection, the spatial diffusion process is discretized and iterated over 20,000 numerical steps to achieve a target smoothing factor of 25.0. During the subsequent normalization of the smoothed image, a numerical floor parameter of $\varepsilon_L = 2 \times 10^{-4}$ is introduced to maintain numerical stability and prevent singularities when evaluating logarithms for the gradient thresholds. The structural parameters tuned to project the drawings into a boolean mask were set to $c_0 = 0.15$ for the intensity lower bound, $c_1 = 0.05$ for the log-gradient upper threshold, and $c_2 = 0.0035$ for the Laplacian ridge selection.

For the local curvature calculation, the interactions are bounded within a finite square submask of 151×151 pixels. This matrix dimension was explicitly chosen to safely exceed the lengthscale required by the inverse spacescale parameter, fixed at $\beta = 0.002$. The topological validation of the connected regions within these submasks – to verify the localized presence of continuous curves – is handled by the scikit-image module.

Finally, because the algorithm computes local integrals and topological evaluations for every valid point in a massive grid, the computational load is substantially heavy. To mitigate this, the implementation utilizes the joblib library alongside Python's native multiprocessing module. This design parallelizes both the image preprocessing steps and the discrete curvature analysis across multiple CPU cores, effectively rendering the execution time manageable for high-resolution archaeological datasets.

5.3 *Discussion*

We adopted the mathematical definition of curvature as a first observable in the description of the style of Roman Corinthian capitals. This is based on the single spacescale parameter β, which represents a strong approximation in the description as in general architectural shapes and ornaments can be distributed on a wide range of spacescales within the same artifact. However, an extension to a multiscale approach appears to be challenging at present. An advantage of our approximation integral is that it does not require regressions, optimizations, or training data. We made the Python implementation public and hope to attract interest in the computational archaeology community.

The algorithm that processed the data from the two Corinthian capitals taken as samples worked on a graphical basis, that is, on a specially prepared two-dimensional representation. The analysis is therefore limited to the evaluation of the outline of the individual constituent elements, and in particular the outline of the acanthus leaves at the base of the *calathos*. Leaving aside the depth dimension, the operator does not detect in the leaves the concavity of the lobes and the overhang of the upper ends, nor the overhang of the decorations carved between *summa folia* and *abacus*: all elements that obviously have considerable relevance in assessing the relative or absolute chronology of the artifacts. In spite of these limitations, we believe that the algorithm can be profitably used for an initial relative serialisation of capitals; especially of capitals pertaining to the later production, where the effect that can be described as 'optical' – resulting from the combination of geometric shadows created between acanthus leaves reduced to stylized forms – is predominant. It is possible, however, that the appropriately trained operator could, in a more advanced version, also detect the third dimension, making typological and stylistic analysis more accurate; and that not only a sequence of 'before' and 'after' could be derived, but also an absolute dating, linking certain formal solutions to similar forms found in capitals datable on external criteria (primarily the chronology of the buildings in which they are employed).

A possible continuation of this work could be to extend the pipeline of curvature estimation to start directly from raw images beyond the special case of drawings. In this direction, the feasibility of studying the curvature on digital 3D models of ancient Roman capitals could be investigated (Empler 2018; Grosman *et al.* 2022), as indeed the 2D projection given by the drawings is an approximate rendering of the shapes' curvature in three-dimensional space.

6. Conclusions and observations on the impact on archaeological field research

The application of this quantitative method to the study of Roman Corinthian capitals could have significant implications for both archaeological research and heritage management. By relying on measurable geometric features such as the curvature of ornamental elements – particularly the acanthus leaves – the method makes it possible to move beyond purely qualitative stylistic assessments and toward a more reproducible analytical framework. As demonstrated in the study, curvature can function as a proxy for stylistic sharpness and formal simplification, two characteristics that evolve noticeably throughout the chronological development of Roman Corinthian capitals. The integration of this approach into digital image processing pipelines could enable the development of tools capable of automatically identifying, from two-dimensional drawings or bidimensional images, the probable chronological range of Roman Corinthian capitals. Such tools would be particularly valuable in museum contexts, where large deposits of architectural fragments remain only partially catalogued or studied. Automated or semi-automated recognition systems could assist curators and researchers in sorting, grouping, and preliminarily dating fragments, thereby accelerating documentation and facilitating comparative analysis across collections. In many cases, museum storerooms contain thousands of architectural elements whose detailed study requires extensive time and specialist expertise. A computational tool capable of quickly identifying stylistic affinities or chronological indicators from images could therefore function as an initial screening mechanism, helping to prioritize objects for further examination and improving the efficiency of cataloguing and research workflows.

In addition, this method may prove especially useful in contexts where cultural heritage is at risk, such as regions affected by conflict, environmental degradation, or uncontrolled development. The ability to rapidly analyse drawings, photographs or scans of architectural fragments and obtain preliminary chronological or typological indications could support emergency documentation and heritage monitoring efforts. In such situations, rapid identification tools can help authorities and researchers record threatened artifacts before they are damaged, displaced, or lost. This capacity has broader social significance, as the preservation and documentation of cultural heritage contribute to safeguarding collective memory, strengthening cultural identity, and ensuring that archaeological knowledge remains accessible to future generations.

More broadly, the method represents a step toward the integration of computational analysis within archaeological practice, enabling scalable and objective approaches to the study of architectural decoration while still complementing the interpretative expertise of specialists. By translating stylistic features into quantifiable parameters, it allows large corpora of artifacts to be analysed systematically, revealing patterns that may be difficult to detect through traditional qualitative observation alone. This does not replace the role of the archaeologist or architectural historian; rather, it provides an additional analytical layer that can support and refine scholarly interpretation. In the long term, the integration of such computational tools may encourage new forms of interdisciplinary collaboration between archaeologists, historians of architecture, computer scientists, and data analysts. It may also facilitate the creation of shared digital repositories in which comparable datasets of architectural drawings, photographs, or 3D models can be analysed using common metrics. Through these developments, computational methods have the potential to expand the scale and precision of research on ancient architectural decoration, while preserving the critical interpretative role of human expertise.

Andrea Auconi, Luigi Sperti, Guido Caldarelli, Myriam Pilutti Namer
Alessandro Codello
Università Ca' Foscari, Venezia
andrea.auconi@unive.it, luigi.sperti@unive.it, guido.caldarelli@unive.it
myriam.piluttinamer@unive.it, alessandro.codello@unive.it

Software

The Python code of the developed estimation method is open access at https://github.com/AndreaAuconi/Capitellum.

Acknowledgements

All authors contributed to the definition of the research objectives, the analytical work, and the discussion of the results. In compliance with the requirements of the Italian academic system for non-bibliometric sectors, Luigi Sperti is responsible for Section 2 and Myriam Pilutti Namer for Section 6.
This publication was supported by the European Union – Next Generation EU – Project PE00000020 – CHANGES – Cultural Heritage Active Innovation for Sustainable Society, CUP H53C22000850006.

REFERENCES

Bello S.M., Soligo C. 2008, *A new method for the quantitative analysis of cutmark micromorphology*, «Journal of Archaeological Science», 35, 6, 1542-52 (https://doi.org/10.1016/j.jas.2007.10.018).

Empler T. 2018, *3D modeling of an archeological area: The imperial fora in Rome*, in M. Rossi, G. Buratti (eds.), *Computational Morphologies: Design Rules Between Organic Models and Responsive Architecture*, Cham, Springer, 185-195.

Freyberger K.S. 1990, *Stadtrömische Kapitelle aus der Zeit von Domitian bis Alexander Severus: zur Arbeitsweise und Organisation Stadtrömischer Werkstätten der Kaiserzeit*, Mainz am Rhein, von Zabern.

Ghosh S., Das N., Das I., Maulik I. 2020, *Understanding deep learning techniques for image segmentation*, «ACM Computing Surveys (CSUR)», 52, 4, 1-35 (https://doi.org/10.1145/33297).

Grosman L. 2016, *Reaching the point of no return: The computational revolution in archaeology*, «Annual Review of Anthropology», 45, 1, 129-145 (https://doi.org/10.1146/annurev-anthro-102215-095946).

Grosman L., Muller A., Dag I., Goldgeier H., Harush O., Herzlinger G., Nebenhaus K., Valetta F., Yashuv T., Dick N. 2022, *Artifact3-d: New software for accurate, objective and efficient 3d analysis and documentation of archaeological artifacts*, «PLoS One», 17, 6, e0268401 (https://doi.org/10.1371/journal.pone.0268401).

Heijmans H. 1995, *Mathematical morphology: A modern approach in image processing based on algebra and geometry*, «SIAM Review», 37, 1, 1-36 (https://doi.org/10.1137/1037001).

Heilmeyer W.-D. 1970, *Korinthische Normalkapitelle: Studien zur Geschichte der römischen Architekturdekoration*, Heidelberg, Kerle.

Herzlinger G., Goren-Inbar N., Grosman L. 2017, *A new method for 3d geometric morphometric shape analysis: The case study of handaxe knapping skill*, «Journal of Archaeological Science: Reports», 14, 163-173 (https://doi.org/10.1016/j.jasrep.2017.05.013).

Hossain M.D., Chen D. 2019, *Segmentation for Object-Based Image Analysis (OBIA): A review of algorithms and challenges from remote sensing perspective*, «ISPRS Journal of Photogrammetry and Remote Sensing», 150, 115-134 (https://doi.org/10.1016/j.isprsjprs.2019.02.009).

Hÿtch M., Hawkes P.W. 2020, *Morphological Image Operators*, Boston, Academic Press.

Karatzas I., Shreve S. 1991, *Brownian Motion and Stochastic Calculus*, New York, Springer.

Kautzsch R. 1936, *Kapitellstudien. Beiträge zu einer Geschichte des Spätantiken Kapitells im Osten vom Vierten bis ins Siebente Jahrhundert*, Berlin, De Gruyter.

Kramer J. 1997, *Spätantike Korinthische Säulenkapitelle in Rom: bei s. Paolo Fuori Le Mura, s. Maria in Domnica und Andere*, Wiesbaden, Reichert.

Leymarie F., Levine M.D. 1989, *Shape Features using curvature morphology*, in W.A. Pearlman (ed.), *Visual Communications and Image Processing IV*, 1199, 390-401 (https://doi.org/10.1117/12.970050).

Leymarie F., Levine M.D. 1993, *Tracking deformable objects in the plane using an active contour model*, «IEEE Transactions on Pattern Analysis and Machine Intelligence», 15, 6, 617-634 (https://doi.org/10.1109/34.216733).

Morgan C. 2022, *Current digital archaeology*, «Annual Review of Anthropology», 51, 1, 213-31 (https://doi.org/10.1146/annurev-anthro-041320-114101).

Pensabene P. 1973, *Scavi di Ostia: I Capitelli. VII*, Roma, Istituto poligrafico dello Stato.

Pensabene P. 1986, *La decorazione architettonica, l'impiego del marmo e l'importazione di manufatti orientali a Roma, in Italia e in Africa (II-VI d.C.)*, Roma-Bari, Laterza.

Pralong A. 2000, *La typologie des chapiteaux corinthiens tardifs en marbre de Proconnèse et la production d'Alexandrie*, «Revue Archéologique», 81-101.

Risken H. 1996, *The Fokker-Planck Equation*, New York, Springer.

Zollt T. 1994, *Kapitellplastik Konstantinopels vom 4. bis 6. Jahrhundert n. Chr.: mit einem Beitrag zur Untersuchung des Ionischen Kämpferkapitells*, Bonn, Habeln.

ABSTRACT

This article proposes a quantitative approach to the stylistic analysis of ancient Roman Corinthian capitals through computational image processing. The study focuses on the evolution of the canonical Corinthian capital produced in Rome and its related contexts between the late first century BCE and the fourth century CE, a period during which significant formal transformations affected the morphology of the acanthus leaves and the overall decorative system. While traditional archaeological analysis has identified several diagnostic features for classification and dating, these assessments have largely relied on the qualitative expertise of specialists. In this work we introduce a basic quantitative method to estimate the curvature of two-dimensional representations of capitals, such as archaeological drawings. The method extracts geometric information from the contours of decorative elements without requiring training datasets or complex machine-learning procedures. By analysing the sharpness and curvature of ornamental features, the approach provides a quantitative descriptor of stylistic change over time. The results demonstrate that this method can distinguish capitals belonging to different chronological phases and therefore has the potential to support archaeological classification, facilitate the study of large corpora of artifacts, and contribute to the development of computational tools for cultural heritage research and documentation.